Scientific Research Publishing

Advances in Materials Physics and Chemistry, 2025, 15(4), 61-73
https://www.scirp.org/journal/ampc
ISSN Online: 2162-5328
ISSN Print: 2162-531X

Multifunctional Smart Nanocomposite Based on Aluminum Oxide Nanopowder and Sialon

Zviad Kovziridze, Natela Nizharadze, Maia Mshvildadze, Tamar Loladze, Gulnazi Tabatadze, Nino Darakhvelidze, Maia Balakhashvili, Marina Kapanadze

Bionanoceramics and Nanocomposite Materials Science Center, Institute of Bionanoceramics and Nanocomposite Technology, Faculty of Chemical Technology and Metallurgy, Georgian Technical University, Tbilisi, Georgia
Email: kowsiri@gtu.ge

How to cite this paper: Kovziridze, Z., Nizharadze, N., Mshvildadze, M., Loladze, T., Tabatadze, G., Darakhvelidze, N., Balakhashvili, M. and Kapanadze, M. (2025) Multifunctional Smart Nanocomposite Based on Aluminum Oxide Nanopowder and Sialon. *Advances in Materials Physics and Chemistry*, **15**, 61-73.
https://doi.org/10.4236/ampc.2025.154004

Received: March 20, 2025
Accepted: April 26, 2025
Published: April 29, 2025

Abstract

Goal: Production of a nanocomposite with high impact strength and crack resistance. **Method:** SiALON with porosity of 13% - 15% was synthesized at 1400˚C using the metallothermic and reactive sintering methods in a nitrogen atmosphere. It was then SiAlON milled in an attritor and in composition with aluminium oxide nanopowder (Table 1), hot pressed and received nanocomposite in the Al_2O_3-SiAlON system. Aluminum oxide nanopowder with an average dispersion of 435 nanometers, produced by the German ALCOA company, was used. For the technology and research, hot pressing was used at 1650˚C. Thermal treatment was conducted for 40 minutes, under pressure 30 MPa, with an 8-minute hold at the final temperature. Studies were performed using micro- and macromechanical methods, as well as structural-optical methods with an AmScope MT300 3.1 MP and electron microscopy techniques. The structural-morphological and elemental composition analysis of the samples was performed using a scanning electron microscope (SEM) JSM-6510LV from the Japanese company JEOL, equipped with an energy-dispersive X-ray spectrometer (EDX) X-MaxN from the British company OXFORD INSTRUMENTS. **Result:** The obtained material is characterized by high operational properties. A dense material with a water absorption rate of 0.O1%, and total porosity—0.13 % was obtained. The bending strength is 470 MPa, while the compressive strength is 1923 MPa. Micro-mechanical analysis showed that no cracks are formed in the sialon matrix during the loading process. **Conclusion:** The high operational properties of the composite were confirmed through the application of Kovziridze's formulas: the dependence of the mechanical modulus and macromechanical properties on the content of the porous phase in the matrix, and the determination of micro- and macromechanical properties, depending on the content of the crystalline phase in the matrix.

Keywords

Nanocomposite, Micro- and Macromechanical Properties, Structure, Reactive Sintering, Hot Pressing

1. Introduction

There are several types of sialons: α, β, X, O1, H, R [1]-[4]. They can be used in oxidizing environment up to 1300˚C and in protective environment up to 1800˚C [5]-[7]. Among these diverse types of sialons, they primarily exist in three phases: α-sialon, β-sialon, and amorphous or partially crystallized phases at the grain boundaries. α- and β-sialons are characterized by unique properties, exhibiting higher hardness and toughness compared to conventional silicon nitride. The α-sialon phase is characterized by higher hardness than the β-sialon phase. β-sialon, like conventional silicon nitride, is distinguished by its higher impact strength. Ceramics, in general, are characterized by high hardness and wear resistance but tend to be brittle. Therefore, our focus was more on the β-sialon phase to obtain a composite with relatively higher impact strength and crack resistance. This is precisely why the composite was chosen to be produced using aluminosilicate raw materials through reaction sintering in a nitrogen atmosphere by the alumino-thermic method, which ensures the formation of the β-sialon phase at a lower temperature compared to the other methods.

2. Main Part

The material composition of the research object is provided in **Table 1**.

Table 1. Material composition of the research object.

The material composition of the CN-8 composite, wt.%								
Name	Geopolymer							
	Kaolin Prosianaya (Ukraine, f/c)	Pologi clay (Ukraine)	Al	Al_2O_3	Si	Perlite (Armenia)	MgO	Y_2O_3
CN-8	13.9	4.63	23.15	27.78	25.00	2.78	0.92	1.8

The chemical composition of the Pologi clay (wt.%) is: SiO_2—47.92, Al_2O_3—35.20, Fe_2O_3—2.06, CaO—0.40, MgO—0.30, and firing loss—12.24. The refractoriness is 1710˚C - 1730˚C.

The chemical composition of kaolin (wt.%) is: SiO_2—46.45, TiO_2—0.33, Al_2O_3—38.70, Fe_2O_3—0.46, MgO—trace, CaO—0.36, Na_2O—0.45, K_2O—0.60, Loss on ignition—13.63. Refractoriness—1770˚C.

A detailed description of the composite preparation is provided in the works [8]-[23]. The phase analysis of the consolidated sample after hot pressing is presented in **Figure 1**.

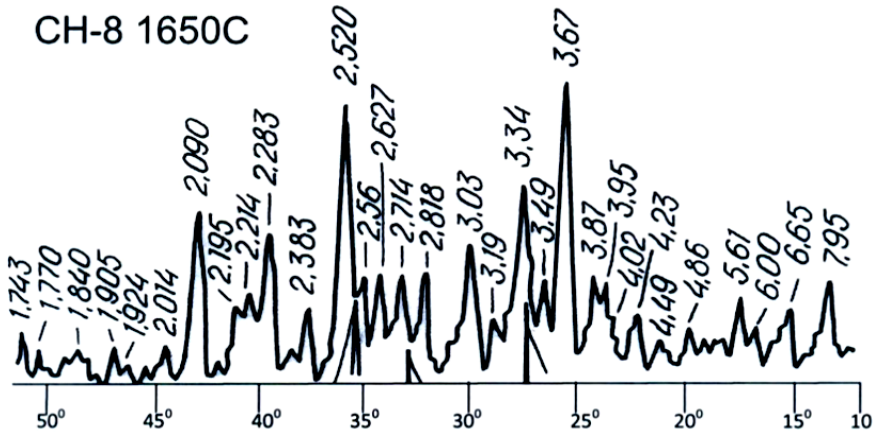

Figure 1. X-ray of the CN-8 composite obtained by hot pressing.

As shown in Figure 1, the X-ray diffraction pattern of the CN-8 composite clearly exhibits the characteristic reflections of sialon—dhkl: 6.65; 5.45; 3.87; 3.67; 2.520; 2.21. Additionally, the diffraction maxima characteristic of corundum are observed—dhkl: 3.49; 2.52; 2.36; 2.09, which were introduced into the phase composition to reinforce the sialon phase.

The physical and technical properties of the obtained samples were studied. The results are presented in Table 2.

The porosity and density of the samples were determined using the hydrostatic weighing method, while the compressive and bending strengths were measured on a 2054 P5 brand testing machine. The obtained results (Table 2) indicate that the samples of the composite, with the selected composition, obtained by hot pressing at 1650˚C and 30 MPa pressure, are consolidated, and the phase composition aligns with the intended goal, as confirmed by the electron microscopy studies. Figure 2 presents the electron microscope image of the fracture surface of the CN-8 composite obtained at 1650˚C.

Table 2. Physical and technical properties of the CH-8 composite obtained by hot pressing at 1600˚C and 1650˚C.

Name of the composite	Open porosity w, %	Total porosity, П, %	Density ρ, g/cm^3	Compressive strength limit, $\sigma_{press.}$, MPa	Bending strength limit, $\sigma_{bend.}$, MPa	Hardness (Vickers), HV, GPa
CN-8 (1600˚C)	0.7	2.49	3.17	1614	456	16
CN-8 (1650˚C)	0.01	0.13	3.21	1923	470	19

The compressive and flexural strength was measured using a German-made tensile testing machine, model R-100, which is equipped to determine the strength limits of samples under compression and three-point bending. The loading rate was 5 mm/min. The compression test was conducted in accordance with GOST 27034-86 (ISO 4506-79). Flexural testing of the ceramic materials was carried out according to GOST 20019-74. In determining the flexural strength limit, the max-

imum stress was calculated using the following formula:

$$\sigma_f = 3/2 \cdot Pl/bh^2$$

where:

- **P** is the force at which the sample fractures (kg)
- **l** is the distance between the supports in three-point bending (mm)
- **b** is the width of the cross-section of the sample (mm)
- **h** is the height of the sample under compression (mm)

The sample was a bar with a square cross-section, length l = 35 mm, width b = 5 mm, height h = 5 mm, and the distance between support points was 25 mm.

As seen from Figure 2, the composite consists of two solid phases: fine corundum particles arranged in the sialon matrix, with the porous phase also represented by a small number of fine pores.

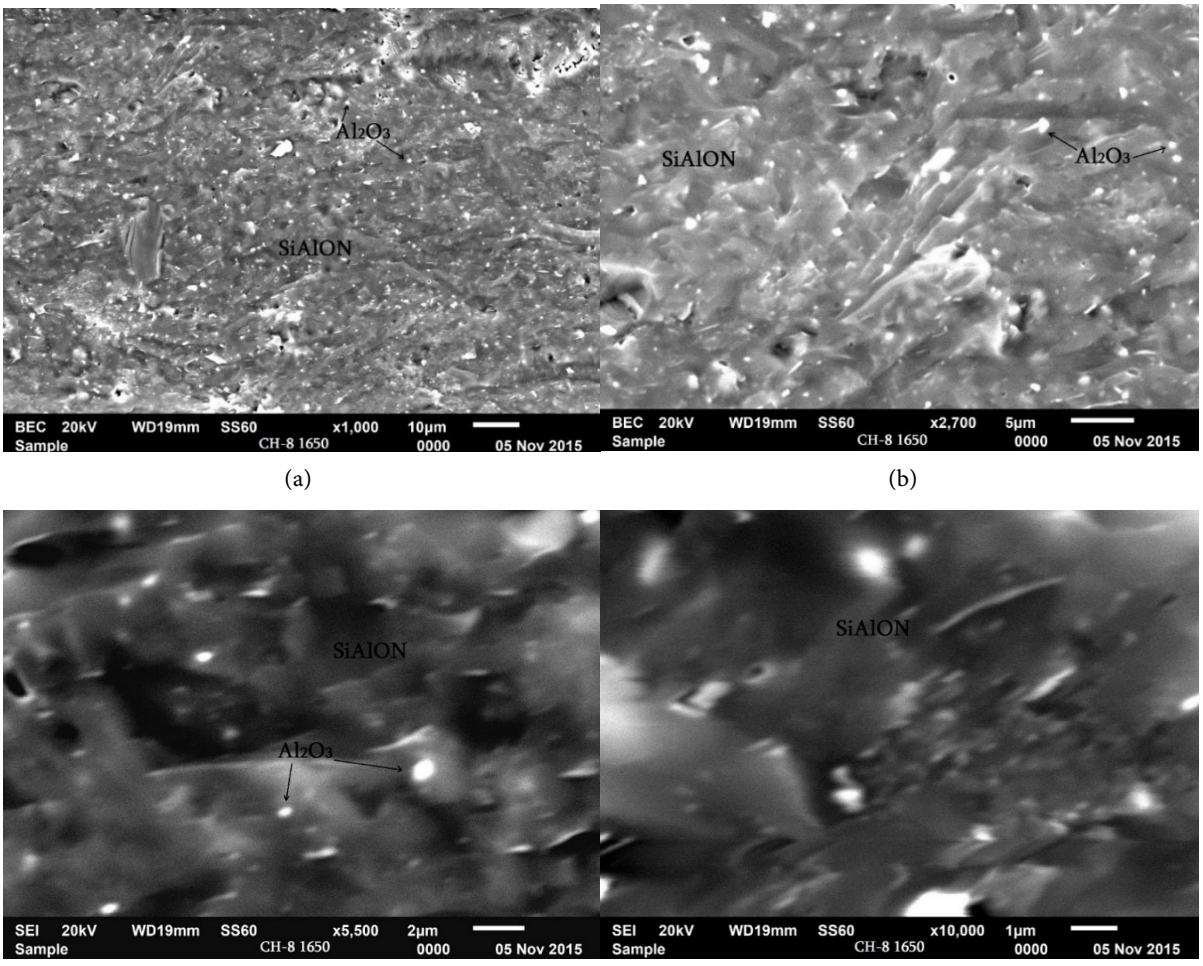

Figure 2. Electron microscope images of the fracture surface of the CN-8 composite obtained at 1650˚C.

The fracture images clearly show that the material exhibits a plastic failure behavior, with cracks forming in the sialon phase. The propagation of these cracks is limited both by the sialon and the finest corundum nano-particles.

The pores are mainly rounded, and the average pore diameter has been calculated (Table 3). The total volume of closed pores reaches 1.58%, which shows a slight difference from the pore volume determined by the hydrostatic method, which can be attributed to measurement inaccuracies inherent in each method. No penetrable or semi-penetrable pores are observed in the matrix. Based on the morphological images, the distribution of pores in the material is both uniform and non-uniform. It is assumed that the pore distribution factor in the matrix, according to Z. Kovziridze's formula, is 0.9.

Table 3. Pore PHASE analysis.

composite **CN-8**	Viewing area S, μm^2	Calculated number of pores, n	Maximum pore size $D_{max.}$ μM	Minimum pore size $D_{min.}$ μM	Pore size $D_{mid.}$ μM	Pore content, %
	345	8	2.0	0.2	0.4	1.98
	345	10	2.0	0.15	0.38	1.17
Average	345	18	2.0	0.15	0.4	1.58

The formula of Z. Kovziridze was used to calculate the dependence of the macromechanical properties of the obtained composite on the porous phase in the matrix.

$$\sigma_{m/p} = \frac{P}{P_m \cdot F_p \cdot P_d \cdot P_{vol}}.$$

Where P is the load, MPa; F_p —the form factor of the pores; P_d —the distribution factor of pores in the matrix. This value is equal to 1, and its value depends on the researcher, based on the morphological image. Depending on how the pores are distributed in the material and their size, the value of this factor can range from 1 to 0.8 If the pores are evenly distributed in the matrix and are approximately of the same size, the factor will be equal to 1. The factor is equal to 0.9 if the pore distribution is uneven, and finally, it is equal to 0.8 if the coalescence[1] process of the pores has started. $P_{vol.}$—the volumetric fraction of the porous phase in the matrix; P_m—the middle size of the pores.

$$\sigma_{m/p} = \frac{470}{0.4 \times 1.58 \times 0.9 \times 13.3} = \frac{470}{7.56} = 62.2 \text{ MPa}$$

The average pore size is 0.855, taken from the sample fired at 1650˚C: 0.13, equal to the value obtained by the hydrostatic weighing method and the visual analysis of the electron microscopy images—1.58 mass%.

2.1. Crystalline Phase Content and Average Sizes

The sizes and content of corundum grains in various visual fields were determined, and the corundum phase content in the composite was calculated (Table

[1]Coalescence—the growth of pores in a solid body, accompanied by a reduction in their total surface area while maintaining the overall volume. The process of pore coalescence is observed in the final stages of sintering and is characterized by the increase in the size of larger pores due to the vacancy dissolution of smaller pores.

4). The actual content of corundum grains may be higher, as the resolution of the finest corundum grains is limited. Given that the mixture contained perlite, the composite also incorporates a certain amount of glassy phase. Non-expanding perlite consists entirely of glassy material (96% by mass of glass, with the remainder consisting of plagioclase, pores, and volatile substances), which melts at 1240˚C [24].

It is likely that the addition of 2.78 mass% perlite to the composition results in the formation of eutectic melts with the geopolymer constituents, particularly with alkaline oxides, thereby increasing the content of the glassy phase V_{gph} in the material. Its content was found to be 6.5%. The glassy phase content was calculated from the same electron microscopy image without the crystalline phase content and pores. Therefore, the amount of crystalline phase should be

$$100 - (V_{ph}{}^{2} + V_{gph}) = 100 - (0.8 + 6.5) = 92.7\%,$$

92.7% the crystalline phase was calculated from the electron microscopy image, based on the size of the microstructural elements and the number of grains.

The content of the SiAlON phase will be 92.7 − 23.5 = 69.2%. As for the size of the SiAlON grains, its structure is represented in the form of layered packets and appears as a continuous matrix in the visual field.

Table 4. Content of corundum grains in the composite.

Composite CN-8	Phase	Viewing area S, μm²	Calculated number of grains, n	Maximum grain size $D_{max.}$ μm	Minimum grain size $D_{min.}$ μm	Average grain size $D_{mid.}$ μm	Phase content %
	Al_2O_3	22.22	32	1.00	0.25	0.50	23.1
	Al_2O_3	30.55	39	1.50	0.20	0.49	23.9
	Average	23.88	3.55	1.5	0.20	0.495	23.5

The microspectral analysis of composite samples was performed, and the results align with those from X-ray and electron microscopy analyses. The findings of the micro X-ray structural analysis are shown in **Figures 3(a)-(d)**.

The correlation[3] between the influence of the crystalline phase and the micro- and macromechanical properties of the materials was calculated using Z. Kovziridze's formula [25].

$$\sigma_{d} = \frac{\text{P. Fkd}}{\text{.Km Kv Fkf}},$$

Where **P** is the load; $\mathbf{K_m}$ is the average size of the crystals; $\mathbf{K_v}$ is the volumetric fraction of crystals in the matrix; $\mathbf{F_{kd}}$ is the distribution factor of the crystals within the matrix, determined by the researcher. It equals 1 for uniform distribution and 0.9 for non-uniform distribution. $\mathbf{F_{kf}}$ is the shape factor of the crystals, defined as the ratio of the largest characteristic dimension of the crystal to the smallest. This

[2]Vphph—Volume of the porous phase.

[3]Correlation—A linear relationship between random events. The measure of correlation is the empirical correlation coefficient. In scientific literature, correlation refers to a statistically significant relationship between parameters of different processes. This definition of the term is not rigid.

allows for the characterization of the shape of the crystal ensemble.

Since the volumetric fraction of crystals in the matrix is very high and equals to 92.7 wt.%, the distribution factor $\mathbf{F_{kd}}$ was assumed to be 1. The average crystal size $\mathbf{K_m}$ for aluminum oxide is 0.495 μm. The size of the sialon crystals could not be measured due to the indistinctness of their boundaries. Visually, the combined average size of the sialon and aluminum oxide crystals was estimated to be 2.5 μm. In this study, the shape factor for aluminum oxide crystals, which exhibit a rounded morphology, was assigned a value of 1. In contrast, sialon crystals, characterized by their elongated shape, were assigned a shape factor of 2.5. Consequently, the overall shape factor for the material system was determined to be 2.5.

$$\sigma_d = \frac{470 \times 1}{2.5 \times 92.7 \times 2.5} = 0.811.$$

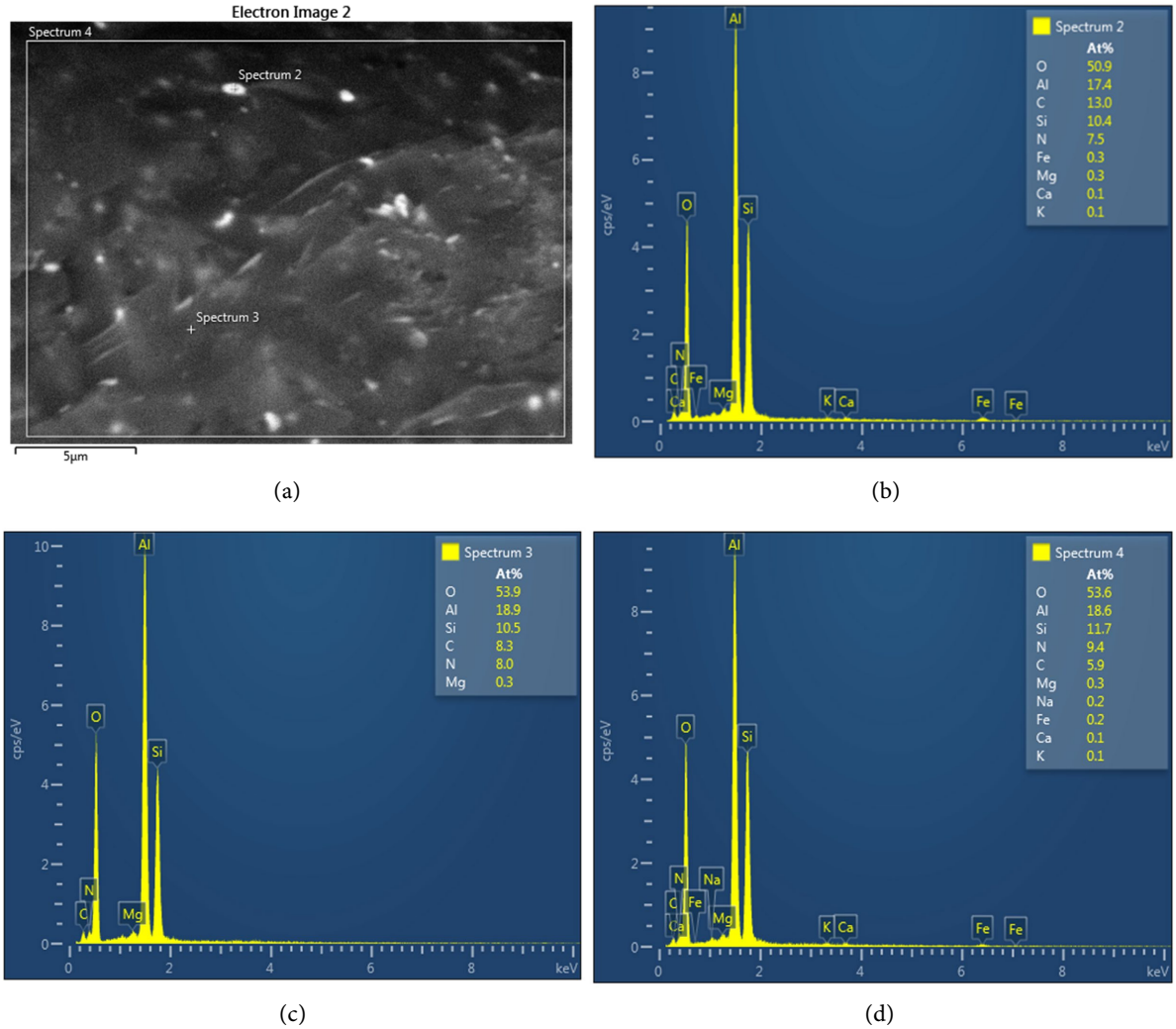

Figure 3. Results of the microspectral analysis of the CN-8 composite obtained at a temperature of 1650˚C.

As the results indicate, there is a high correlation, which is understandable

since the content of the crystalline phase is high, the degree of crystal dispersion is also high, and the result is achieved by the even distribution of the phase within the matrix. The primary phase component in the matrix is the crystalline phase.

The dynamic hardness and elastic modulus of the obtained composite were determined using the dynamic ultramicrohardness tester DUH-211S, in accordance with the requirements of the modern international standard ISO-14577.

Dynamic hardness (DH) is determined by the applied load on the indenter and its penetration depth into the material. Unlike traditional static methods, this approach accounts for both plastic and elastic components. The results are independent of indentation size, applied loads, and variations in elastic recovery. Dynamic hardness was measured in a load-unload regime prior to elastic relaxation. The results are shown in Table 5.

Table 5. Micromechanical properties of the CN-8 composite obtained at a temperature of 1650˚C.

<<*** Test condition-CH8-1650 ***>>			
Test mode	Load-unload		
Sample name	CH8-1650	Sample No.	CH8-1650
Test force	200.00 [mN]	Minimum force	1.96 [mN]
Loading speed	1.0 (70.0670 [mN/sec])	Hold time at load	5 [sec]
Hold time at unload	3 [sec]	Test count	3
Parameter name		Parameter	20
Comment	24.11.15. .SH8-1650-Tex-Uni-200		
Poisson's ratio	0.250		
Cf-Ap, As Correction	ON	Indenter type	Vickers
Read times	2	Objective lens	50
Indenter elastic	1.140e+006 [N/mm^2]	Indenter poisson's ratio	0.070

<<*** Test result ***>>

SEQ	Fmax [mN]	hmax [um]	hp [um]	hr [um]	DHV-1	DHV-2	Eit [N/mm2]	Length [um]	HV	Data name
1	206.11	1.2419	0.4801	0.6795	666.193	4435.000	9.252e+004	4.517	1910.017	CH8-1650 (1)
2	210.42	1.3860	0.6371	0.8510	546.009	2550.168	8.182e+004	4.517	1949.885	CH8-1650 (2)
3	206.11	1.2701	0.6173	0.7663	636.923	2659.186	9.501e+004	4.517	1910.001	CH8-1650 (3)
Average	207.55	1.2993	0.5782	0.7656	616.375	3214.785	8.979e+004	4.517	1923.301	
Std. Dev.	2.484	0.076	0.085	0.086	62.672	1058.143	7007.244	0.000	23.023	
CV	1.197	5.879	14.783	11.204	10.168	32.915	7.804	0.000	1.197	

The analysis of the indenter impressions after microhardness measurements is presented in Figure 5.

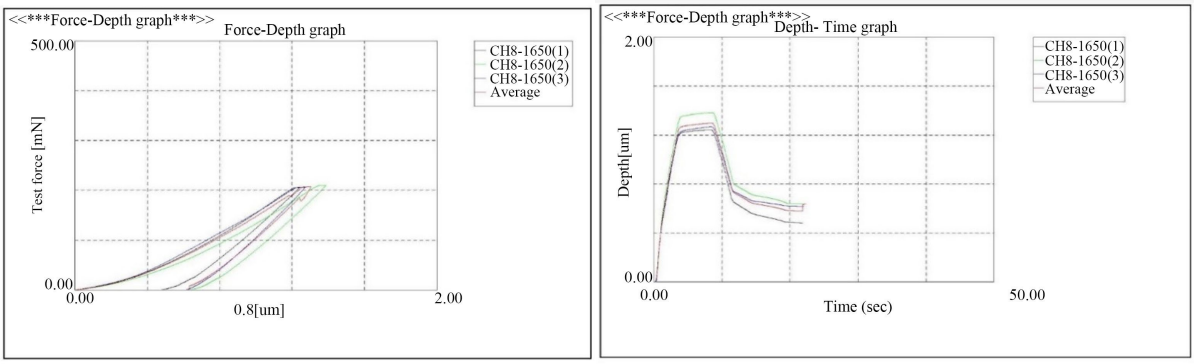

(a) (b)

Figure 4. Micromechanical properties of the CN-8 composite under a 2 mN load: (a) Depth of indenter penetration over time; (b) Load on the indenter as a function of indentation depth.

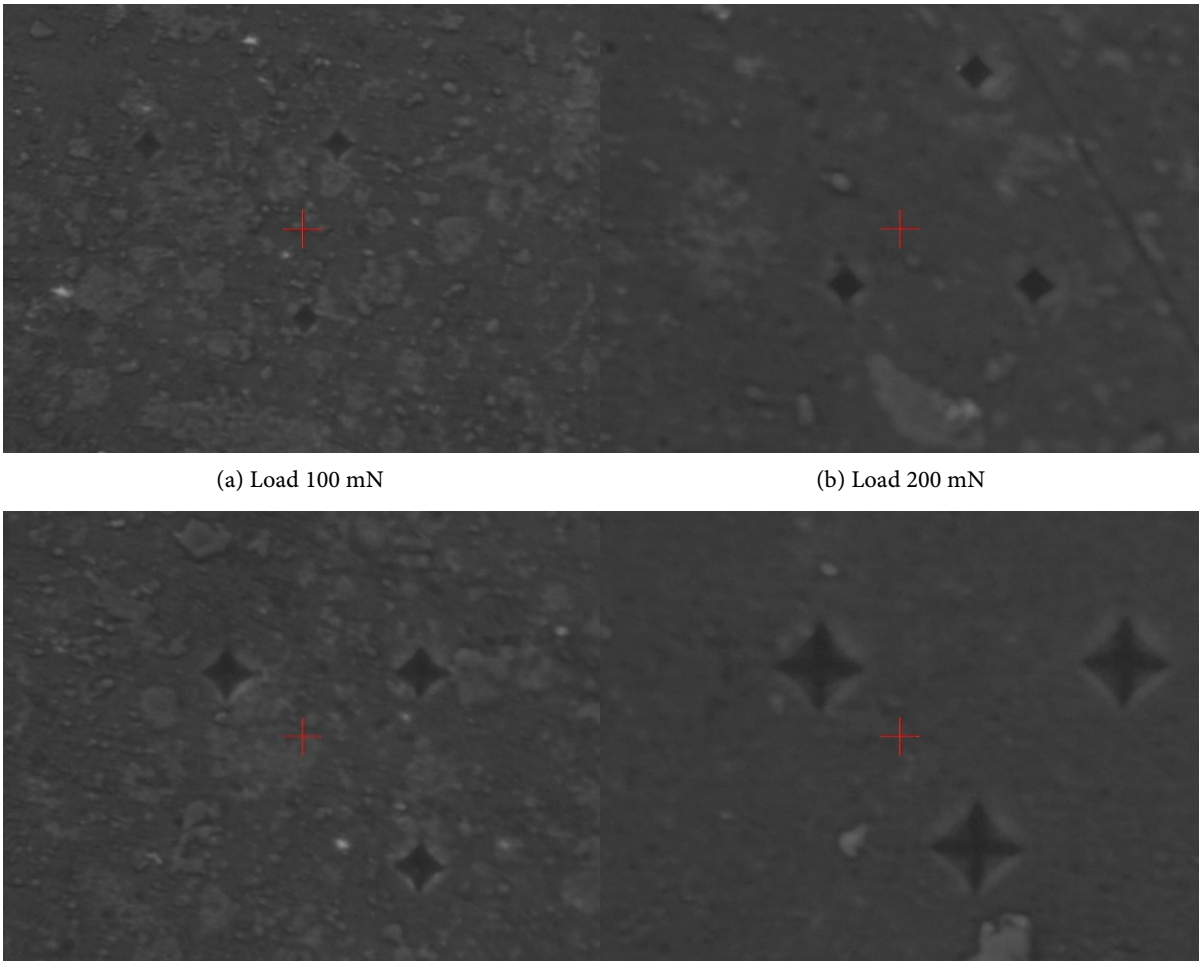

(a) Load 100 mN (b) Load 200 mN

(c) Load 300 mN (d) Load 500 mN

Figure 5. Indenter impressions at different loads.

As shown in **Figure 4**, the boundaries of the indentations are well-defined, and even at a load of 1000 mN, no crack is observed, indicating the high crack resistance of this composite.

The prevention of crack propagation can be experimentally achieved by regulating both the material composition and the thermal treatment regime. In our case, this resulted in enhanced mechanical properties. As Griffith and Oravan pointed out in their works, every sintered material contains microscopic cracks, ranging from 2 to 9 weight%. Interestingly, a low level of closed porosity can positively affect the material's mechanical performance, as the stresses generated within the matrix are distributed evenly across these pores, allowing the ceramic to maintain high mechanical strength.

Table 6. Average sizes of impressions and cracks.

Indentation image number and load value, mN	Indentation depth in the material, h, μM	Indentation diagonal length, a, μm	Half of the indentation Diagonal a/2, μm	Average crack Length ℓ, μM	Note
(a) 100	0.8200	3,546	1.773	Crack is not detected.	Indentation is made on the matrix
(b) 200	1.2993	4,517	2.258	Crack is not detected.	Indentation is made on the matrix
(c) 300	1.8168	6,412	3.206	Crack is not detected.	Indentation is made on the matrix
(d) 500	2.8475	8,452	4.226	Crack is not detected.	Indentation is made on the matrix

In our case, crack propagation is further hindered by the dominant presence of the strongest constituent phase, the crystalline phase, which features fine grains uniformly distributed throughout the matrix. Additionally, the uniform distribution of small pores and their low content, as observed in electron microscopy images, plays a crucial role. While the potential for crack propagation under thermal stress, especially during cooling, always exists, the aforementioned conditions effectively counteract these harmful processes.

Mechanical Modulus of the Materials

The mechanical modulus of the material was calculated using the formula for the modulus proposed by Kovziridze [26]:

$$M = \frac{Kvol.E.Kic.Pd}{Km.Gvol..Pvol..Pm} MPa/\mu M^2,$$

Where Kvol is the volume fraction of the crystalline phase in the material (%); E is the modulus of elasticity (MPa); Kic is the critical stress intensity factor; Pd is the factor for the distribution of pores in the matrix, which is taken as 1 for uniform distribution, 0.9 for non-uniform distribution, and 0.8 for pore coalescence; Km is the average size of crystals in the matrix (μm); Gvol is the content of the glassy phase in the matrix (%); Pvol is the volume fraction of pores in the matrix (%); Pm is the average size of pores in the matrix (μm). The units of the modulus are $MPa/\mu m^2$. The formula does not account for Griffith's cracks [27] [28], dislocations in crystals, or nano-defects in the glass, but it provides a comprehensive representation of the material's resistance to external loading, closely approximating

the calculated values of atomic bond strength. This is why the modulus of elasticity is included in the formula:

$$M = 92.7 \times 8.987 \times 40.75 \times 0.9/2.5 \times 6.5 \times 0.855 \times 0.4$$
$$= 30184.6/7.6 = 5.45 \text{ GPa}/\mu M^2.$$

The cited literature provides extensive literature data on materials containing sialon. Thus, a means of comparative analysis is provided in the literature.

3. Conclusions

The composite in the Al_2O_3-SiAlON system was synthesized using a metallothermic and nitrogen-assisted reactive sintering method. To obtain a dense material, the porous (13% - 15%) composite was finely ground in an attritor, then hot-pressed at 1650˚C. Subsequent investigations were carried out using micro- and macromechanical methods, as well as structural-optical and electron microscopy techniques. The porous phase was examined, and its percentage content and size were determined, along with the percentage content and grain sizes of the crystalline components—silicon nitride and aluminum oxide.

The results of the study indicate that β-sialon with a silicon nitride structure has been obtained. The process is facilitated by the presence of an imperfect crystalline phase of newly formed silicon nitride at lower temperatures, which, due to its relatively large porosity, incorporates aluminum oxide and aluminum nitride into the structure. Subsequently, at higher temperatures of 1350˚C - 1450˚C, the β-sialon structure is formed.

The obtained material exhibits high operational properties. The bending strength is 470 MPa, while the compressive strength is 1923 MPa. Micromechanical analysis showed that no crack forms in the sialon matrix during the loading process.

The composite's high operational properties were confirmed by calculating the mechanical modulus using Kovziridze's method, with the obtained result exceeding expectations. This modulus allows for a realistic assessment of the material's resistance to external loading. The material was obtained by solid-phase sintering.

The composite was also tested using Z. Kovziridze's formula—the relationship between macromechanical properties and the content of the porous phase in the matrix.

To determine the micro- and macromechanical properties as a function of the crystalline phase content in the matrix, Kovziridze's formula was also used. A high correlation of 0.811 was obtained.

Conflicts of Interest

The authors declare no conflicts of interest regarding the publication of this paper.

References

[1] Ekström, T., Käll, P.O., Nygren, M. and Olsson, P.O. (1989) Dense Single-Phase B-Sialon Ceramics by Glass-Encapsulated Hot Isostatic Pressing. *Journal of Materials*

Science, **24**, 1853-1861. https://doi.org/10.1007/bf01105715

[2] Rosenflanz, A. and Chen, I. (1999) Phase Relationships and Stability of α'-SIALON. *Journal of the American Ceramic Society*, **82**, 1025-1036. https://doi.org/10.1111/j.1151-2916.1999.tb01869.x

[3] Strelov, K.K. (1996) Theoretical Foundations of Refractory Materials Technology: A Textbook for Universities. 2nd Edition.

[4] Kovziridze, Z. and Darakhvelidze, N. (2022) Obtaining Multifunctional Ceramic Composite Materials Based on a Silicone Matrix, Using Cheap Raw Materials and Simplified Innovative Technology. 100*th Anniversary of* "*Georgian Technical University-GTU*", Tbilisi, Georgia, 24-26 June 2022, 1065-1076.

[5] Zheng, G., Zhao, J., Gao, Z. and Cao, Q. (2011) Cutting Performance and Wear Mechanisms of Sialon-Si_3N_4 Graded Nano-Composite Ceramic Cutting Tools. *The International Journal of Advanced Manufacturing Technology*, **58**, 19-28. https://doi.org/10.1007/s00170-011-3379-2

[6] Tressler, R.E. (1994) Theory and Experiment in Corrosion of Advanced Ceramics. In: *NATO Science Series E*: (*Closed*), Springer, 3-23. https://doi.org/10.1007/978-94-011-1182-9_1

[7] Piekarczyk, J., Lis, J. and Bialoskórski, J. (1993) Elastic Properties, Hardness and Indentation Fracture Toughness of β-Sialons. *Key Engineering Materials*, **89**, 541-546. https://doi.org/10.4028/www.scientific.net/kem.89-91.541

[8] Kovziridze, Z., Nizharadze, N., Darakhvelidze, N., Tabatadze, G. and Mestvirishvili, Z. (2014) Carbon and Aluminothermic Processes Occurring in a Nitrogen Atmosphere Based on Geopolymer. *Journal of the Georgian Ceramic Society* "*Ceramics*", **16**, 32-36.

[9] Kovziridze, Z., Nizharadze, N., Darakhvelidze, N., *et al.* (2014) Sialon Production via Nitroaluminothermic Processes. *Journal of the Georgian Ceramic Society* "*Ceramics*", **16**, 23-31.

[10] Darakhvelidze, N., Kovziridze, Z., Nizharadze, N., Tabatadze, G. and Mestvirishvili, Z. (2022) High Temperature Multifunctional Heteromodulus Nano Composite for Armor Plates, Turbine Disk and Fan, Refractory and Wear-Resistant Aggregates. *Moambe Bulletin of the Georgian National Academy of Sciences*, **16**, 32-37.

[11] Kovziridze, Z., Nizharadze, N., Tabatadze, G., *et al.* (2022) Obtaining and Study Smart Composites in the B_4C-SiC-Si-Al-Al_2O_3-Carbon Fiber System Advances in Materials Physics and Chemistry. *Advances in Materials Physics and Chemistry*, **12**, 323-337. https://doi.org/10.4236/ampc.2022.1211021

[12] Kovziridze, Z., Nizharadze, N., Darakhvelidze, N., Tabatadze, G. and Mestvirishvili, Z. (2016) Sialon-Containing Composite Production via Nitro Aluminothermic Processes, Reactive Sintering, and Hot-Pressing Methods. *Journal of the Georgian Ceramic Society*, **18**, 9-19.

[13] Kovziridze, Z., Nizharadze, N., Tabatadze, G., Darakhvelidze, N., Balakhashvili, M., *et al.* (2022) Obtaining and Study Smart Composites in the B_4C-SiC-Si-Al-Al_2O_3-Carbon Fiber System. *Journal of the Georgian Ceramists Association Ceramics and Advanced Technologies*, **24**, 63-78.

[14] Kovziridze, Z., Nijaradze, N., Daraxvelidze, N., Tabatadze, G., *et al.* (2017) Preparation of Composites by Nitro Aluminothermic Processes, over β-SiAlON Matrix in the SiAlON-SiC-Al_2O_3 System. *Journal of Electronics Cooling and Thermal Control*, **6**, 62-77.

[15] Kovziridze, Z., Nizharadze, N., Qinqladze, V. and Darakhvelidze, N. (2023) High

Refractory Composites on the Basis of Silicon Carbide. *Journal of the Georgian Ceramists Association Ceramics and Advanced Technologies*, **25**, 38-48.

[16] Kovziridze, Z., Nizharadze, N., Darakhvelidze, N., *et al.* (2017) Composite Production via Metallothermic and Nitriding Processes in Si-SiC-Al Geopolymer Systems. *Journal of the Georgian Ceramic Society*, *Ceramics and Advanced Technologies*, **19**, 33-52.

[17] Kovziridze, Z., Nijaradze, N., Tabatadze, G., Cheishvili, T., Mshvildadze, M., Mestvirishvili, Z., *et al.* (2017) Obtaining of Sialon Composite via Metal-Thermal and Nitrogen Processes in the Sic-Si-Al-Geopolymer System. *Journal of Electronics Cooling and Thermal Control*, **7**, 103-122. https://doi.org/10.4236/jectc.2017.74009

[18] Kovziridze, Z., Nijaradze, N. and Danelia, T. (2023) Smart Nanocomposite in the Al_2O_3-TiC System. *Proceedengs Book of Tokyo 7th International Innovative Studies and Contemporary Scientific Congress*, 21-23 April 2023, Tokyo Japan, 262-270.

[19] Kovziridze, Z., Nizharadze, N., Darakhvelidze, N., *et al.* (2018) Sialon-Containing Composite Production via Reactive Sintering Method in SiC-B_4C-Si-Al-Al_2O_3 Systems through Metallothermic and Nitriding Processes. *Journal of the Georgian Ceramic Society*, *Ceramics and Advanced Technologies*, **20**, 13-17.

[20] Kovziridze, Z., Nizharadze, N., Darakhvelidze, N., Tabatadze, G. and Mestvirishvili, Z. (2019) Study of the Phase Composition of Composites in the SiC-B_4C-Si-Al-Al_2O_3 System. *Journal of the Georgian Ceramic Society*, *Ceramics and Advanced Technologies*, **21**, 44-51.

[21] Kovziridze, Z. and Danelia, T. (2023) Preparation of Hetero-Modular Nanocomposites Based on the B_4C-SiC-BN-TiC-Al_2O_3 System for Turbine Disks and Wings, Ballistic Armor, for Working in Hot Nodes of FLYING machines. *Journal of the Georgian Ceramists Association*, *Ceramics*, *Science and Advanced Technologies*, **25**, 49-62.

[22] Kovziridze, Z., Nizharadze, N., Tabatadze, G., Cheishvili, T., and Darakhvelidze, N. (2024) Multifuctional Nanocomposites in B_4C-TiC-TiB_2-SiC-BN-Al_2O_3-SIALON-C Carbon Fiber System For Armor Fillets, Turbine Disks and Wings, High-Temperature Wear Resistant Nodes. *International Journal of Multidisciplinary Research and Analysis*, **7**. https://doi.org/10.47191/ijmra/v7-i05-51

[23] Kovziridze, Z., Nijaradze, N., Tabatadze, G., Cheishvili, T., Mshvildadze, M., Kapanadze, M., Balakhashvili, M. and Daraxvelidze, N. (2024) Smart Nanocomposite in the SiC-Si-Al-Al_2O_3-Geopolymer System. *International Journal of Innovative Research in Multidisciplinary Education,* **3**, 1121-1136. https://doi.org/10.58806/ijirme.2024.v3i6n28

[24] Kovziridze, Z.D. (1993) Development of the Scientific Fundamentals and Technology for Producing Celestine and Aluminosilicate Ceramics Using Barite and Perlite. Dissertation for the Degree of Doctor of Technical Sciences, Tbilisi.

[25] Kovziridze, Z. (2020) The Formula of Dependence of Mechanical Characteristics of Materials on Crystalline Phase Composition in the Matrix. *Advances in Materials Physics and Chemistry*, **10**, 178-188. https://doi.org/10.4236/ampc.2020.108013

[26] Kovziridze, Z. (2017) Formula for the Mechanical Modulus of Ceramic Materials and Composites. National Intellectual Property Center of Georgia "Sakpatenti".

[27] Griffith, A.A. (1924) The Theory of Rupture. *Proceedings of the First International Congress for Applied Mechanics*, 55-63.

[28] Orowan, E. (1933) Die Zugfestigkeit von Glimmer und das Problem der technischen Festigkeit. *Zeitschrift fur Physik*, **82**, 235-266. https://doi.org/10.1007/bf01341490